Chin. J. Astron. Astrophys. Vol. 8 (2008), No. 5, 591–602
(*http://www.chjaa.org*)

Chinese Journal of
Astronomy and
Astrophysics

Modeling ϵ Eri and Asteroseismic Tests of Element Diffusion *

Ning Gai[1,3], Shao-Lan Bi[2,1] and Yan-Ke Tang[1,3]

[1] National Astronomical Observatories / Yunnan Observatory, Chinese Academy of Sciences, Kunming 650011, China; *gaining@ynao.ac.cn*
[2] Department of Astronomy, Beijing Normal University, Beijing 100875, China
[3] Graduate School of Chinese Academy of Sciences, Beijing 100049, China

Received 2007 November 7; accepted 2008 March 26

Abstract Taking into account the helium and metal diffusion, we explore the possible evolutionary status with a seismic analysis, of the MOST (Microvariability and Oscillations of STars) target: the star ϵ Eri. We adopt different input parameters to construct models to fit the available observational constraints in, e.g., $T_{\rm eff}$, L, R and [Fe/H]. From the computation we obtain the average large spacings of ϵ Eri to be about $194 \pm 1\,\mu$Hz. The age of the diffused models was found to be about 1 Gyr, which is younger than the age determined previously by models without diffusion. We found that the effect of pure helium diffusion on the internal structure of the young low-mass star is slight, but that of metal diffusion is obvious. The metal diffusion leads the models to have much higher temperature in the radiative interior, and, correspondingly a higher sound speed there, hence a larger frequency and spacings.

Key words: stars: evolution — stars: interiors — stars: individual: ϵ Eridani

1 INTRODUCTION

Element diffusion, sometimes named "atomic" diffusion, is a basic physical transport mechanism of elements driven by pressure (or gravity), temperature and composition gradients. The effects of helium diffusion on the structure of solar models were first studied by Noerdlinger (1977). Later, this process was effectively studied by helioseismology (Guenther et al. 1993; Guenther 1994; Bahcall & Pinsonneault 1992b; Christensen-Dalsgaard et al. 1993; Guenther & Demarque 1997). Recently, results from the helioseismic studies have demonstrated that models that incorporate element diffusion are in substantially better agreement with the inferred sound speed than models that do not.

Up to date, the effect of element diffusion has been tested by asteroseismic method in solar type stars. Vauclair & Théado (2004), Théado et al. (2005) and Castro & Vauclair (2006) have presented discussions of asteroseismic signatures of pure helium diffusion in main-sequence stars between 1.1 $M_\odot$ and 2.0 $M_\odot$, in terms of the "second differences". In the present work, we shall study the effects of both helium and metal element diffusion on models with masses less than 1 $M_\odot$.

Metals could affect the temperature gradient and the convection in the star's envelope. It also leads to variations in the central temperature, density, pressure and radiative opacity. Thus, it is important to consider the influence of the metals on the star's internal structure. Here, we investigate the effects of metal diffusion on the structure, evolution and oscillation frequency of the late K-type star, ϵ Eri.

The bright K2V dwarf, ϵ Eri (HD 22049, HIP 16537, HR 1084, PLX 742), is one of the nearest solar-like stars, at a distance of about 3.218 pc. It has a planetary companion, ϵ Eri b (Hatzes et al. 2000). Its proximity makes this planetary system a prime target for future extrasolar planet direct–imaging efforts and

* Supported by the National Natural Science Foundation of China.

for the study of the process of formation of planetary systems. The success of these efforts will depend on the mass and age of the system. Therefore, the study of the exoplanet – host star, ϵ Eri, is a key issue.

A number of authors have carried out theoretical analysis to determine precise global parameters of ϵ Eri (Guenther & Demarque 1986; Guenther 1987; Soderblom & Däppen 1989) (hereafter GD 86, G87 and SD 89 respectively). Thanks for the work of Noyes et al. (1984), which measured the p-mode oscillation spectrum of ϵ Eri and identified three individual frequencies in the power spectrum between 1500 μHz and 2000 μHz with average large spacing of 172$\pm$5 μHz. Based on non-asteroseismic and asteroseismic observational constraints, GD 86, G87 and SD 89 constructed a series of stellar models of ϵ Eri. However, in these works, there is a contradiction between the young age implied by the high chromospheric activity and rapid rotation rate on one hand, and the old age implied by the slightly metal-poor composition, on the other. GD 86, G87 and SD 89 discussed this contradiction and gave the ages of 12 Gyr, 10 Gyr and 1 Gyr, respectively.

Recently, evidence from many observations seems to indicate that ϵ Eri is a young main-sequence star with age less than 1 Gyr. For example, Song et al. (2000) derived an age of 0.73 $\pm$ 0.2 Gyr, using the Li abundance together with the star's position in the H-R diagram and kinematics; Di Folco et al. (2004) estimated an age of 0.85 Gyr from measurement of its radius by long-baseline interferometry; Saffe et al. (2005) used the calibrations of Donahue (1993) and Rocha-Pinto & Maciel (1998) (with a correction for the effect of chromospheric activity) to derive estimated ages of 0.66 Gyr and 0.82 Gyr, respectively. The SIMBAD database gives the age of ϵ Eri as 0.66 Gyr.

We aim to provide a basic theoretical study of ϵ Eri. We will use the latest interferometric observational radius (Di Folco et al. 2004) to constrain the stellar models and to predict the frequency spacings. Then, we will investigate the effects of helium and metal diffusion on the internal structure and, hence, on the frequency spacings.

In Section 2 the global parameters of the star are summarized. The input physics, computing method and results of analysis are summarized in Section 3. The helium and metal diffusion effects on the stellar models, and the oscillation frequency are checked in Section 4. Finally, conclusions are presented in Section 5.

2 OBSERVATIONAL CONSTRAINTS

It is difficult observationally to determine accurately the mass of stars except in some cases of binary systems. As a single star, ϵ Eri has various values of mass published in the literature, e.g., 0.85$\pm$0.04 $M_\odot$ (Santos et al. 2001), 0.80 $M_\odot$ (Minier & Lineweaver 2006), 0.82 $M_\odot$ (Takeda et al. 2005) and 0.83 $M_\odot$ (Fischer & Valenti 2005).

For the effective temperature of ϵ Eri, we adopt $T_{\rm eff}$ = 5012 $\pm$ 67, which was determined using the infrared flux method (IRFM) (Ramírez & Meléndez 2004).

The luminosity can be calculated from the absolute visual magnitude $M_{\rm v}$ = 6.18 $\pm$ 0.11 (Song et al. 2000; Takeda et al. 2005). Given the bolometric correction $B.C.$ = – 0.28 (Takeda et al. 2005), the absolute bolometric magnitude is $M_{\rm bol}$ = $M_{\rm v}$ + $B.C.$ = 5.9 $\pm$ 0.11. Then the luminosity is computed by the formula: $M_{\rm bol}$ = –2.5log$(L/L_\odot)$ + $M_{\rm bol,\odot}$. Adopting $M_{\rm bol,\odot}$ = 4.746, we then obtain $\log\,(L/L_\odot)$ = – 0.4176 $\sim$ – 0.5056.

Compared with the Sun, ϵ Eri is slightly metal-poor. Santos et al. (2004) obtained [Fe/H] = – 0.13 $\pm$ 0.04 from a spectroscopic analysis based on 39 FeI and 12 FeII lines. In order to deduce $[Z/X]$, we assume that the logarithm of $[Z/X]$ is proportional to the abundance ratio [Fe/H] (Thoul et al. 2003):

$$\log[Z/X]_{\rm star} = [{\rm Fe/H}]_{\rm star} + \log[Z/X]_\odot\,, \tag{1}$$

where $[Z/X]_\odot$ = 0.023 (Grevesse & Sauval 1998). Using this ratio, we obtain $[Z/X]_{\rm surf}$ = 0.017 $\pm$ 0.0016.

The initial helium mass fraction of the star, Y_i, is important for determining its structure, but Y_i of ϵ Eri is unknown observationally. GD 86 and G87 adopted Y_i to be 0.236 and SD 89 considered Y_i to be from 0.24 to 0.26. In view of these values, we shall, in the present study, adopt an initial helium abundance of Y_i = 0.245$\pm$0.015.

The large spacings sensitively depend on the radius. For predicting the large spacings that will be observed by MOST (Microvariability and Oscillations of STars), we take the latest interferometric observational radius $R/R_\odot$ = 0.734 $\pm$ 0.01 (Di Folco et al. 2004).

Table 1 Observational Parameters of ϵ Eri

Parameters	ϵ Eri	Ref
$M/M_\odot$	0.85 ± 0.04	(1)
	0.80	(2)
	0.82	(3)
	0.83	(4)
$[\mathrm{F_e/H}]_{\mathrm{surf}}$	-0.13 ± 0.04	(5)
$R/R_\odot$	0.743 ± 0.010	(6)
M_{v}	6.18 ± 0.11	(7)
	6.18	(3)
$\log(L/L_\odot)$	-0.4616 ± 0.044	(8)
T_{eff}(K)	5012 ± 67	(9)

(1) Santos et al. (2001); (2) Minier & Lineweaver (2006); (3) Takeda et al. (2005); (4) Fischer & Valenti (2005); (5) Santos et al. (2004); (6) Di Folco et al. (2004); (7) Song et al. (2000); (8) this paper; (9) Ramírez & Meléndez (2004).

3 MODELING OF THE STAR

3.1 Input Physics

The evolutionary models are computed using the version of Yale stellar evolution code (Guenther et al. 1994) that was modified to include the effects of element diffusion. The initial zero-age main sequence (ZAMS) models was calculated from pre-main sequence evolution which were assumed to have spherical symmetry, no rotation and no magnetic field. In the computation we used the OPAL equation of state tables EOS2001 (Rogers & Nayfonov 2002), the opacities with a smooth blend of OPAL GN93 (Iglesias & Rogers 1996) and OPAL tables (Alexander & Ferguson 1994). The relevant nuclear reaction rates and cross sections are from Bahcall & Pinsonneault (1992a, b) and Bahcall (1989). Considering ϵ Eri is a solar-like star, we chose the Krishna-Swamy (1966) atmosphere model. The diffusion of both helium and metal element abundance was included in the stellar model computation, by using the coefficients of Thoul et al. (1994).

Using the standard mixing-length theory, we set α = 1.7 for all models, which is close to the value required to reproduce the solar radius under the same physical assumptions and stellar evolution code (Murphy & Demarque 2004). If rotation and magnetic field are neglected in the construction of stellar model, convection is the most important mechanism that is usually included in standard stellar models which describes material motions within a star especially for low-mass main sequence star. The convective overshoot is another factor influencing the chemical composition of the star. The change of mixing-length parameter α would also influence principally the radius of the base of the outer convection zone. The presence of core overshoot would extend the core-burning phase of evolution and increase the estimated age of star. This important topic has been studied separately by Bi et al. (2008). However, the element diffusion could also lead to the redistribution of the element in star and change the depth of the convective envelope (Guenther 1994).

3.2 Element Diffusion

Element diffusion in stars is driven by the gravitational setting, temperature gradients, composition gradients and radiation pressure, as was shown in detail by Bahcall & Pinsonneault (1992a). The gravity and temperature gradients tend to concentrate the helium and heavier elements toward the center of the star, while the hydrogen diffuses outward, but the concentration gradients work in the oppose direction. In addition, radiation pressure can cause partially ionized or neutral species to rise relative to species with smaller cross sections. However, radiation pressure is efficient in the external regions of main-sequence stars with $T_{\mathrm{eff}} > 6000\,\mathrm{K}$ (Michaud 1976). So the diffusion caused by radiative pressure is tiny in K-type stars and will be neglected in this paper.

3.2.1 Basic Equation for Element Diffusion

Most studies on chemical diffusion use either the method of Chapman - Enskog (Chapman & Cowling 1970) or the method of Burgers (1969) for deriving the transport properties from the Boltzmann equation. In our work the element diffusion is described using the equations of Burgers (1969) with the diffusion velocity coefficients from Thoul et al. (1994). A single model includes both helium and metal element diffusion. The change rate of the element mass fractions due to the diffusion is now written as (Thoul et al. 1994; Bahcall & Loeb 1990):

$$\frac{\partial X_s}{\partial t} = -\frac{1}{\rho r^2}\frac{\partial[r^2 X_s T^{5/2}\xi_s(r)]}{\partial r}\,, \tag{2}$$

where the partial derivatives are evaluated in the local rest frame of the mass shell inside the star, ρ, r, T are the local values of density, radius, temperature, and X_s is the mass fraction of the element s.

The diffusion velocity for species s is defined by

$$w_s = \frac{T^{5/2}\xi_s}{\rho}, \tag{3}$$

and the function $\xi_s(r)$ has the expression,

$$\xi_s(r) = A_p(s)\frac{\partial \ln p}{\partial r} + A_{\rm T}(s)\frac{\partial \ln T}{\partial r} + \sum_{c\neq e,2} A_{\rm c}(s)\frac{\partial \ln C_c}{\partial r}\,. \tag{4}$$

In Equation (4), A_p, $A_{\rm T}$, $A_{\rm c}$ correspond to the gravitational setting, thermal diffusion and concentration gradient diffusion, respectively, and are functions of the mass only. The suffix c refers to all species other than helium.

3.2.2 Treatment of Diffusion in the Evolutionary Code

The Yale stellar evolution code has been modified to include the effects of He diffusion from gravitational settling and thermal diffusion (Bahcall & Pinsonneault 1992a) using the method of Bahcall & Loeb (1990) and with the metal diffusion added in 1994. The method by which element diffusion is treated in a standard stellar evolution code has been presented by Bahcall & Pinsonneault (1992a) in detail.

In the diffusion subroutine given by Bahcall & Pinsonneault (1992a), the main task is to solve the diffusion equation and calculate the change of the element abundance by diffusion. Equation (2) can be written in the following form,

$$\frac{dx}{dt} = \frac{1}{\rho r^2}\Big[\frac{d}{dr}(D_1) + \frac{d}{dr}\Big(D_2\frac{dx}{dr}\Big)\Big]\,, \tag{5}$$

where D_1, D_2 are the diffusion coefficients.

For helium diffusion,

$$\left\{\begin{array}{l} D_1(Y) = \frac{F_{\rm gy}\cdot r^2\cdot T^{5/2}}{\ln\Lambda}\cdot\frac{d\ln p}{dr}\cdot X\cdot(A_p^X + A_{\rm T}^X), \\ D_2(Y) = \frac{F_{\rm gy}\cdot r^2\cdot T^{5/2}}{\ln\Lambda}\cdot A_{\rm c}^X, \end{array}\right\} \tag{6}$$

and for metal diffusion,

$$\left\{\begin{array}{l} D_1(Z) = \frac{F_{\rm gz}\cdot r^2\cdot T^{5/2}}{\ln\Lambda}\cdot\frac{d\ln p}{dr}\cdot Z\cdot(A_p^Z + A_{\rm T}^Z), \\ D_2(Z) = \frac{F_{\rm gz}\cdot r^2\cdot T^{5/2}}{\ln\Lambda}\cdot A_{\rm c}^Z. \end{array}\right\} \tag{7}$$

The radius, temperature and density are in the nondimensional units defined by $r = r'/R_\odot$, $T = T'/10^7$ K, $\rho = \rho'/100\,{\rm g\ cm^{-3}}$ and $t = t'/10^{13}$ yr, respectively (Bahcall & Pinsonneault 1992a; Chaboyer et al. 1992).

In Equations (6) and (7), $F_{\rm gy}$ and $F_{\rm gz}$ are adjustable multiplicative factors of the helium and metal diffusion coefficients. In our work, we set both these two factors to 1.0. The exact numerical solution of A_p, $A_{\rm T}$, $A_{\rm c}$ are calculated by an export subroutine developed by Thoul (1994).

Table 2 Model Parameters of ϵ Eridani

Model	A1	A2	A3	B1	B2	B3	C1	C2	C3
	$M/M_\odot = 0.83$ $Z_i = 0.012$ $Y_i = 0.2315$			$M/M_\odot = 0.83$ $Z_i = 0.013$ $Y_i = 0.2365$			$M/M_\odot = 0.83$ $Z_i = 0.014$ $Y_i = 0.2415$		
Dif.	None.	Y.Dif	Y& Z.Dif	None.	Y.Dif	Y& Z.Dif	None.	Y.Dif	Y& Z.Dif
Age(Gyr)	1.151	1.089	1.0	1.206	1.138	1.0	1.264	1.191	1.0
$L/L_\odot$	0.321	0.321	0.321	0.319	0.319	0.319	0.317	0.317	0.317
$R/R_\odot$	0.749	0.750	0.744	0.750	0.751	0.743	0.751	0.753	0.741
$T_{\rm eff}$ (K)	5024.9	5019.8	5039.5	5012.2	5006.7	5036.3	4999.9	4993.8	5033.5
$r_{\rm cz}/R$	0.7073	0.7053	0.7048	0.7046	0.7033	0.7024	0.7024	0.7022	0.7000
$\tau_{\rm cz}$ (s)	1504.8	1514.1	1496.7	1514.4	1522.9	1496.7	1523.2	1529.5	1497.0
τ_0 (s)	2524.5	2532.5	2502.4	2530.1	2538.8	2493.6	2535.7	2545.2	2484.5
$\tau_{\rm cz}(s)/\tau_0(s)$	0.5961	0.5979	0.5981	0.5986	0.5999	0.6002	0.6007	0.6009	0.6025
$\langle\Delta\nu\rangle$	192.2	191.4	193.8	191.6	191.0	194.6	191.2	190.5	195.1

In Equation (5) the partial time derivative is evaluated at constant mass shell of the star. The diffusion equation is solved with zero hydrodynamic velocity of the stellar plasma. In the right hand of Equation (5), the first term depends on the first spatial derivatives of the element mass fraction and the second term on the second spatial derivatives of the element abundance. The first term is solved explicitly using the two-step Lax-Wendroff technique (Press et al. 1986) by neglecting the second derivatives of the element abundance. We then use this trial solution as the initial abundance to determine the second derivatives by a fully implicit method (Bahcall & Pinsonneault 1992a) and so obtain the final updated element abundance.

For the helium diffusion, we only consider the diffusion of ^{4}He and ignore that of ^{3}He (Loeb et al. 1989). The time rate of change of the ^{4}He mass fraction Y is equal in magnitude and opposite in sign to the rate of change of the hydrogen mass fraction.

The diffusion of all metal elements is assumed to proceed at the same rate as fully ionized iron. Because of the diffusion of metal elements, the radiative opacity has to be changed after each time step for each spherical shell. We calculate the effect of metal element diffusion on the opacity by computing the total metal element abundance at each model radius $Z(r)$, and then interpolating for the opacity between opacity tables with different total metal element abundances (Bahcall et al. 1995).

The diffusion subroutine carries out the diffusion calculations using data supplied by other parts of the Yale code, in which the thermal structure and the element abundances are calculated. It is assumed that the amount of diffusion within a given time step is too small to affect significantly the changes in the thermal structure, abundances, and nuclear reaction rates that are calculated elsewhere. After the diffusion computation, we update the element abundance and then calculate the thermal structure.

In the diffusion subroutine, the element diffusion is treated only in the radiation region. The characteristic time for the element to diffuse through a solar radius under solar conditions is of the order of 10^{13} yr (Bahcall et al. 1995), much larger than the age of the sun or ϵ Eri. However, helioseismic inferences have demonstrated the significance of element diffusion (Cox et al. 1989; Bahcall & Loeb 1990; Bahcall & Pinsonneault 1992a; Proffitt 1994).

3.3 Method of Computation and Results of Analysis

3.3.1 Evolutionary Tracks and Candidates for Pulsation

In order to reproduce observational constraints of ϵ Eri, we have computed a grid of evolutionary tracks for six values of $M/M_\odot$: 0.80, 0.81, 0.82, 0.83, 0.84 and 0.85, and for values of the initial metallicity Z_i: 0.011, 0.012, 0.013 and 0.014.

From a series of evolutionary tracks computed, we selected those models that land within the observational constraints in $\log T_{\rm eff}$, $\log L/L_\odot$ and $\log R/R_\odot$ in the H-R diagram. Then we further chose the models on the basis of the constraint of the observed $[Z/X]$. From the computation alone, we note that the age of ϵ Eri is likely to be in the range 0.1 – 1.0 Gyr. Here we consider the age ($\leq$ 1 Gyr) as a property of the star considered in SD 89. According to the age estimated from observation, as given in the introduction, we

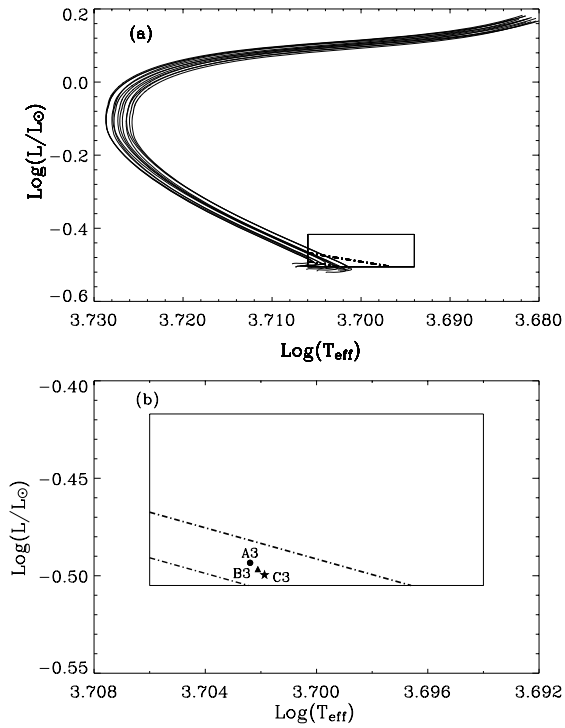

Fig. 1 (a) Evolutionary tracks (12 in total) in the H-R diagram starting from the ZAMS. The solid lines mark the box delimited by the observed luminosity and effective temperature. The two dash dot lines mark the region delimited by the interferometric radius. (b) Enlargement of the error box of panel (a). The models A3, B3 and C3 are denoted by the filled circle, triangle and pentacle, respectively.

constrain the age of models to the range of 0.60 – 1.0 Gyr. We have 12 tracks falling within the observational error box and these are plotted in Figure 1(a).

To deduce the set of parameters that best agrees with the observations, we performed a χ^2 minimization as described in Eggenberger (2005). The χ^2 function is defined as

$$\chi^2 \equiv \sum_{i=1}^{4} \left(\frac{C_i^{\rm theo} - C_i^{\rm obs}}{\sigma} \right)^2 , \tag{8}$$

where the vector $C_i^{\rm obs} \equiv (L/L_\odot, T_{\rm eff}, R/R_\odot, [Z/H]_s)$. The vector $C_i^{\rm obs}$ and the observational error vector σ are given in Table 1. The χ^2 minimization yields three models, A3, B3 and C3, and these are presented in Figure 1(b) and Table 2.

3.3.2 Calibration of Models with and without Diffusion

Based on the selected models A3, B3 and C3, we calibrated three groups of models with mass $M/M_\odot = 0.83$ and different initial chemical compositions. The models of the same group have the same initial chemical compositions, but with different types of element diffusion. See Table 2.

We use the stellar pulsation code of Guenther (1994) to calculate the eigenfrequencies and the large spacings of the models listed in Table 2. For solar-like stars, the eigenfrequencies $\nu_{n,l}$ of oscillation modes, characterized by the radial order n at harmonic degree l, satisfy the simplified asymptotic relation (Tassoul 1980):

$$\nu_{n,l} = \Delta\nu \Big(n + \frac{l}{2} + \alpha + \frac{1}{4} \Big) + \epsilon_{n,l} \, . \tag{9}$$

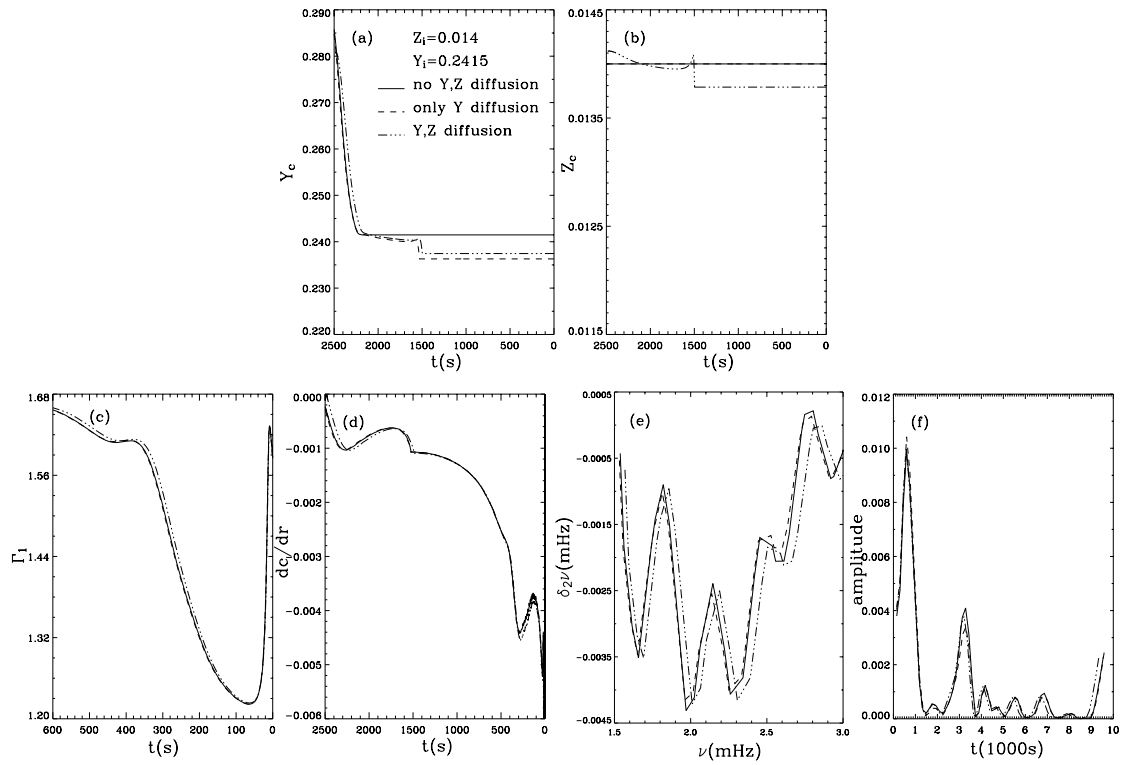

Fig. 2 Stellar structures of the group (C) models in Table 2 with Y_i = 0.2415 and Z_i = 0.014. Solid lines: standard homogeneous model C1 without diffusion; dashed lines: model C2 with pure helium diffusion; dash dot lines: model C3 with both helium diffusion and metal diffusion. (a) Helium profiles as a function of the acoustic depths in the models, i.e. the time for the acoustic waves to travel from the surface down to the considered layer; (b) Metal profiles show a clear gradient at the bottom of the convection zone; (c) Adiabatic exponent Γ_1 profiles show a clear feature at the place of the He_{II} ionization zones; (d) Sound speed gradients in which the dips are clearly visible at the place of the He_{II} ionization zones and the bottom of the convection zones; (e) Second differences of the oscillation frequencies as a function of the frequencies; (f) Fourier transform of panel (e).

The large spacings are defined by the frequencies of the same harmonic degree l and the adjacent radial order n:

$$\Delta\nu_{n,l} \equiv \nu_{n,l} - \nu_{n-1,l} \,. \tag{10}$$

We average the large spacings over the modes l = 0, 1, 2, 3 and n = 10, 11, ..., 30 to obtain the mean value.

From the age of the star in Table 2, we can see that the diffusion could speed up the evolution of stars. The model with both helium and metal diffusion has the smallest age of all the models in the same group. The mean of the large spacings of models A3, B3 and C3 is about 194 $\pm$ 1 μHz. The pure helium diffusion hardly affects $\nu_{n,l}$, but the effect is relatively obvious after adding the metal diffusion. It also seems that the diffusion effect is increase alone with increase of the initial heavy element abundance (Y_i, Z_i).

4 ASTEROSEISMIC TEST, HELIUM AND METAL DIFFUSION EFFECTS

4.1 "Second Differences" Tests, Helium and Metal Gradients

Stellar acoustic p-modes with low l degree can propagate deeply inside the stars. However, as mentioned by Gough (1990), rapid variations of the sound speed inside a star lead to partial reflections of the sound waves. A conveniently and easily evaluated measure of this oscillatory component is the "second differences" with

respect to the radial order n of the frequencies ν_{nl} for the same value of the harmonic degree l:

$$\Delta_2\nu_{nl} \equiv \nu_{n-1,l} - 2\nu_{n,l} + \nu_{n+1,l}\,. \tag{11}$$

This measure is contaminated less than the first difference $\Delta_1\nu_{nl} \equiv \nu_{n,l}$ - $\nu_{n-1,l}$ by the smoothly varying components of $\Delta_1\nu_{nl}$. The modulation in the frequency has been extensively studied in the He$_{\rm II}$ ionization zone and the edge between the convective and radiative zones. In the He$_{\rm II}$ ionization zone there is a rapid variation of the adiabatic exponent Γ_1 and in the base of the convection zone there is essentially a discontinuity in the sound speed gradient, i.e. dc/dr, produced a discontinuity in ν_{nl}. In order to identify the different components which modulate the oscillations, we have computed the Fourier transform of the "second differences". The modulation period of the "second differences" is twice the "acoustic depth" of the region, then we have

$$\tau_s = \int_{r_s}^{R} \frac{dr}{c(r)}\,, \tag{12}$$

where τ_s is the time needed for the acoustic waves to travel between the surface and the considered region (the He$_{\rm II}$ ionization zone or the base of the convection zone), $c(r)$ the sound speed at radius r, and r_s the radius of the considered region.

Vauclair & Théado (2004), Théado et al. (2005) and Castro & Vauclair (2006) showed there are asteroseismic signatures of pure helium diffusion in terms of the "second differences" in stars between 1.1 $M_\odot$ and 2.0 $M_\odot$. They checked the precise signatures on the oscillation frequencies of helium gradients inside stars. In our work we computed stars of 0.83 $M_\odot$ and not only included helium diffusion but also metal diffusion.

Figure 2(a), (b) displays the helium and metal abundance profiles as a function of the acoustic depth in the three models: no element diffusion, pure helium diffusion, and both helium and metal diffusion. Due to the diffusion, helium and metal drift inward and form a gradient just below the convective zone. The acoustic depth of the bottom of the convection zones $\tau_{\rm cz}$ and the corresponding $\tau_{\rm cz}/\tau_0$, τ_0 being the total acoustic depth of the star, are listed in Table 2 for models with different initial chemical compositions and different types of diffusion. Figure 2(c),(d) gives the adiabatic exponent Γ_1 profiles and the sound speed gradients dc/dr versus the acoustic depth. From the dc/dr profiles it is clear that the dips around 300 s and 1500 s are caused by the He$_{\rm II}$ ionization zones and the bottom of the convection zones.

Considering the range of validity of the asymptotic approximation, we select modes of degrees l = 0, 1, 2, 3 and oscillation frequencies between 1500 μHz and 3000 μHz to compute the "second differences". In Figure 2(e)(f) we present the second differences of our models and the Fourier transforms of these curves. We have explained that the modulation period corresponding to the peaks in the Fourier transforms are twice the "acoustic depth" of the region where the feature occurs. By comparing the dips of dc/dr profiles in Figure 2(d) with the Fourier transforms in Figure 2(f), one can recognize the peaks due to the He$_{\rm II}$ ionization zones and those corresponding to the bottom of the convective zones in Figure 2(f).

From the Fourier transforms in Figure 2(f), we can see that the amplitudes of the peaks corresponding to the modulation periods corresponding to the base of the convection zones are different for the models C1, C2, C3. Mazumdar & Antia (2001) showed that the amplitude of the oscillatory signal in the second differences contains an amplification factor of $4\sin^2(\pi\tau_s/\tau_0)$. When $\tau_s/\tau_0 > \frac{1}{2}$, the Fourier transforms show that the peak amplitude decreases with the layer getting deeper (Vauclair & Théado 2004). From the values of $r_{\rm cz}/R$ and $\tau_{\rm cz}/\tau_0$ in Table 2, we find that diffusion could deepen the outer convective zone, especially the metal diffusion. The base of the convective zone is deepest of all in the same group. From the Fourier transforms, we find the peak amplitude at $2\tau_{\rm cz}$ to be lower in the models with pure helium diffusion than in those without diffusion. In term of the amplification factor of $4\sin^2(\pi\tau_s/\tau_0)$, the peak amplitude of models with both helium and metal diffusion should be the lowest of all, but is actually higher than that with pure helium diffusion. So we think that the peak amplitude is mainly determined by the depth of the base of the convection zone, while it is also sensitive to the element gradient at the bottom of convective zone. From Figure 2(b), it is obvious that the metal gradient steepens more rapidly than the helium gradient. Moreover, there is a stronger reflection of sound waves in the region of the metal gradient, that is why the model which contains metal diffusion has a higher amplitude of the peak of $\tau_{\rm cz}$.

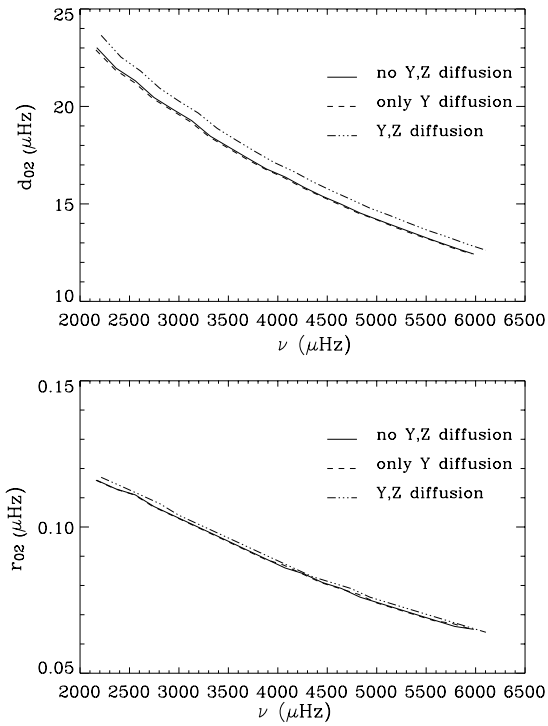

Fig. 3 Upper panel: small spacings $d_{02}(n)$. Lower panel: frequency separation ratios $r_{02}(n)$ for the models in group (C).

4.2 Tests of Internal Structure

The small frequency spacings are given by

$$d_{ll+2}(n) = \nu_{n,l} - \nu_{n-1,l+2}\,. \tag{13}$$

Using the asymptotic theory of p modes it is shown (Christensen-Dalsgaard & Berthomieu 1991; Basu et al. 2007),

$$d_{ll+2}(n) \simeq -(4l+6)\frac{\Delta\nu_{nl}}{4\pi^2\nu_{n,l}}\int_0^R \frac{dc}{dr}\frac{dr}{r}\,, \tag{14}$$

where R is the radius of the star and $\Delta\nu_{nl}$ is the large spacing. Now, in the core the gradient of the sound speed is large and r is small, so the integral in Equation (14) is dominated by the conditions in the core. So the small spacings usually test the stellar core, but the small spacings are also slightly affected by effects near the surface. To reduce the effect of uncertainties in the latter, the frequency separation ratios are used (Roxburgh & Vorontsov 2003),

$$r_{02}(n) = \frac{d_{02}(n)}{\Delta_1(n)}, \qquad r_{13}(n) = \frac{d_{13}(n)}{\Delta_0(n+1)}\,. \tag{15}$$

Each panel of Figure 3 shows the small spacing d_{02} and the frequency separation ratios r_{02} for the different models of group (C) with different types of diffusion as labeled in the figure. We see that the pure helium diffusion hardly alters the internal structure in these young, low–mass models, while metal diffusion makes obvious differences in the internal structure.

We now explore the changes of the internal structure from the asteroseismic test by comparing the internal physical parameters of the models with and without diffusion. It is known that the sound speed

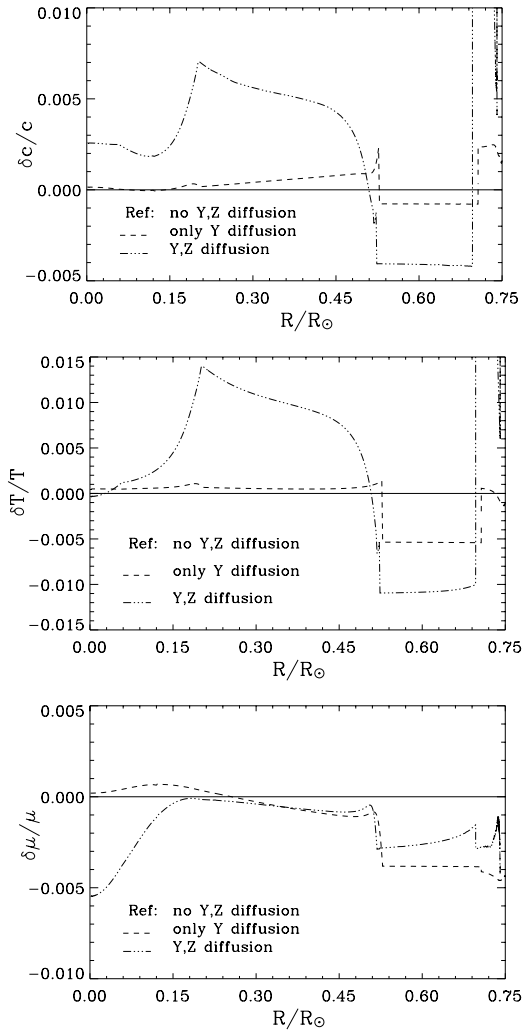

Fig. 4 From top down: Relative sound-speed difference $\delta c/c$, temperature difference $\delta T/T$ and mean molecular weight $\delta\mu/\mu$, respectively, as function of radius, for the models of group (C). All differences are with respect to model C1 of no diffusion. The dashed lines for the model with pure He diffusion (eg., $\delta\mu/\mu$ = ($\mu_{Y.\mathrm{Dif}}$ - $\mu_{\mathrm{None.Dif}}$) / $\mu_{\mathrm{None.Dif}}$). The dash-dot lines for the model with both He and Z diffusion (e.g. $\delta\mu/\mu$ = ($\mu_{Y\&Z.\mathrm{Dif}}$ - $\mu_{\mathrm{None.Dif}}$) / $\mu_{\mathrm{None.Dif}}$).

depends on both the mean molecular weight and the temperature (Basu et al. 2007; Bi et al. 2008),

$$c^2 \simeq \frac{K_B T}{\mu m_u} \propto \frac{T}{\mu}\,. \tag{16}$$

In Figure 4, we show the radial profiles of $\delta c/c$, $\delta T/T$ and $\delta\mu/\mu$. It is seen that the effect of pure helium diffusion on the three parameters is small and hardly alters the values of c, T and μ in the radiation interior, and any effect is concentrated in the convection zone. Due to the diffusion, helium drifts inward just below the convection zone, which makes μ in the envelope smaller. On the other hand, the increase of opacity in the envelope due to the settling of He leads to a lower temperature. However, helium diffusion reduces both the T and μ, and also the sound speed c slightly in the convective envelope. So the small spacings and separation ratios are not much affected by helium diffusion.

In Figure 4 the dash dot lines refer to the differences between the model with both helium and metal diffusion and the model without any diffusion. We see the effect of metal diffusion on c, T and μ not only in the convective envelope but also in the radiative interior. Due to diffusion, helium and metal drift inward just below the convection zone, causing μ to decrease in the outer envelope. Moreover, Z is depleted in the envelope and is enriched in the interior, the opacity increases in the former, and decreases in the latter. It leads to a lower temperature in the envelope and a higher temperature in the interior. Figure 4 shows that, of the three physical parameters considered, the temperature is the most sensitive one to the metal diffusion. Here $\delta c/c$ is mainly dependent on the variation of $\delta T/T$, and the sound speed c is much larger in the interior of the model than in the outer convective envelope. From the sound speed gradient in Equation (16), we have

$$\frac{dc}{dr} \propto \frac{d\left(\frac{T}{\mu}\right)^{1/2}}{dr} = -\frac{1}{2}\left(\frac{T}{\mu^3}\right)^{\frac{1}{2}}\frac{d\mu}{dr} + \frac{1}{2}\frac{1}{(T\mu)^{\frac{1}{2}}}\frac{dT}{dr}\,, \tag{17}$$

and we obtain that the temperature T is the dominate factor in the sound speed gradient in causing the differences between the models with and without metal diffusion. Because dT/dr is negative, $|dc/dr|$ in the radiative interior is larger than in the model without metal diffusion. So from Equation (14), the small spacings are larger than in the other models, which explains the variation of the internal structure including metal diffusion.

5 CONCLUSIONS

Taking into account the effects of helium and metal diffusion on stellar evolution, we presented a detailed modeling of the MOST target, ϵ Eri, subject to the available observational constraints in the effective temperature, luminosity, high precision interferometric observational radius and metallicity. We also consider the age ($\leq$ 1 Gyr) as a constraint on the models, as was done in SD 89.

According to our results, the location of ϵ Eri in the H-R diagram indicates that the star has evolved little since its arrival on the zero-age main sequence. Taking into account the helium and metal diffusion, we find that the mean large spacing, $\langle\Delta\nu\rangle$, averaged over l = 0, 1, 2, 3 and n = 10, 11, 12, ..., 30, is about $194 \pm 1\,\mu$Hz.

In order to test the effect of helium and metal diffusion, we constructed three groups of models with the same mass but different Y_i and Z_i. Then, for the given chemical composition we calibrate three models with different types of diffusion listed in Table 2. In our work we fixed the mixing length parameter α = 1.70 and neglected convective overshoot. The results show that the age of the models with diffusion is about 1 Gyr, and is younger than that determined by the models without diffusion.

Due to the effect of diffusion, helium and metals fall below the outer convective zone and form a gradient. We use the "second differences" to locate the depth of the convective zones. When metal diffusion is considered, the convective zone sinks more quickly and the metal gradient steepens more rapidly than the helium gradient. This induces a stronger reflection of the sound waves just below the convection zone, which explains the higher peak amplitude than in the case of pure helium diffusion, at the base of the convective zone.

Small spacings and frequency separation ratios have been used to test the differences in internal structure between models with and without diffusion. According to our results, pure helium diffusion hardly alters the internal structure in young, low-mass models. Metal diffusion mainly induces a much higher temperature in the radiative interior, hence a higher sound speed in the interior of the model. Correspondingly, frequencies and large spacings are obviously larger than in models without metal diffusion. The difference in internal structure between models with and without metal diffusion increases obviously with increasing initial metallicity. So we conclude that it is necessary to consider metal diffusion in young main-sequence low-mass stars.

Acknowledgements We are grateful to an anonymous referee for his/her constructive suggestions and valuable remarks to improve the manuscript. This work was supported by The Ministry of Science and Technology of China through Grant 2007CB815406, and by the NSFC through Grants 10173021, 10433030, 10773003 and 10778601.

References

Alexander D. R., Ferguson J. W., 1994, ApJ, 437, 879
Bahcall J. N., 1989, Neutrino Astrophysics, Cambridge: Cambridge Univ.
Bahcall J. N., Loeb A., 1990, ApJ, 360, 267
Bahcall J. N., Pinsonneault M. H., 1992a, RvMP, 64, 885
Bahcall J. N., Pinsonneault M. H., 1992b, ApJ, 395, 119
Bahcall J. N., Pinsonneault M. H., Wasserburg G. L., 1995, RvMP, 67, 781
Basu S., Chaplin W. J., Elsworth Y. et al., 2007, ApJ, 655, 660
Bi S. L., Basu S., Li L. H., 2008, ApJ, 673, 1093
Burgers J. M., 1969, Flow equations for composite gases, New York: Academic Press
Castro M., Vauclair S., 2006, A&A, 456, 611
Chaboyer B., Deliyannis C. P., Demarque P. et al., 1992, ApJ, 388, 372
Chapman S., Cowling T. G., 1970, The Mathematical Theory of Non-Uniform Gases, Cambridge Univ. Press
Christensen - Dalsgaard J., Berthomieu G., 1991, in Solar Interior and Atmosphere, Thcson, AZ, University of Arizona Press, 1991, 401
Christensen - Dalsgaard J., Proffitt C. R., Thompson M. J., 1993, ApJ, 403, L75
Cox A. N., Guzik J. A., Kidman R. B., 1989, ApJ, 342, 1187
Di Folco E., Thévenin F., Kervella P. et al., 2004, A&A, 426, 601
Donahue R. A., 1993, Ph.D thesis, New Mexico State Univ.
Eggenberger P., Carrier F., Bouchy F., 2005, NewA, 10, 195
Fischer D. A., Valenti J., 2005, ApJ, 622, 1102
Gough D. O., 1990, LNP, 367, 283
Grevesse N., Sauval A. J., 1998, SSRv, 85, 161
Guenther D. B., Demarque P., 1986, ApJ, 301, 207
Guenther D. B., 1987, ApJ, 312, 211
Guenther D. B., Pinsonneault M. H., Bahcall J. H., 1993, ApJ, 418, 469
Guenther D. B., 1994, ApJ, 422, 400
Guenther D. B., Demarque P., 1997, ApJ, 484, 937
Hatzes A. P., Cochran W. D., McArthur B. et al., 2000, ApJ, 544, 145
Iglesias C. A., Rogers F. J., 1996, ApJ, 464, 943
Krishna Swamy K. S., 1966, ApJ, 145, 174
Loeb A., Bahcall J. N., Milgrom M., 1989, ApJ, 341, 1108
Murphy E. J., Demarque P., Guenther D. B., 2004, ApJ, 605, 472
Mazumdar A., Antia H. M., 2001, A&A, 377, 192
Michaud G., Charland Y., Vauclair S. et al., 1976, ApJ, 210, 447
Minier V., Lineweaver C., 2006, A&A, 449, 805
Noerdlinger P. D., 1977, A&A, 57, 407
Noyes R. W., Baliunas S. L., Belserene E. et al., 1984, ApJ, 285, L23
Press W. H.,Flannery B. P., Teukolsky S. A., 1986, Numerical Recipes, Cambridge: Cambridge Univ.
Proffitt C. R., 1994, AJ, 425, 849
Ramírez I., Meléndez J., 2004, ApJ, 609, 417
Rocha-Pinto H. J., Maciel W. J., 1998, MNRAS, 298, 332
Rogers F. J., Nayfonov A., 2002, ApJ, 576, 1064
Roxburgh I. W., Vorontsov S. V., 2003, A&A, 411, 215
Saffe C., Gómez M., Chavero C., 2005, A&A, 443, 609
Santos N. C., Israelian G., Mayor M., 2001, A&A, 373, 1019S
Santos N. C., Israelian G., Mayor M., 2004, A&A, 415, 1153
Soderblom D. R., Däppen W., 1989, ApJ, 342, 945
Song I., Caillault J. -P., Barrado y Navascués D. et al., 2000, ApJ, 533, L41
Takeda Y., Ohkubo M., Sato B. et al., 2005, PASJ, 57, 27
Tassoul M., 1980, ApJS, 43, 469
Théado S., Vauclair S., Castro M. et al., 2005, A&A, 437, 553
Thoul A. A., Bahcall J. N., Loeb A., 1994, ApJ, 421, 828
Thoul A. A., Scuflaire R., Noels A. et al., 2003, A&A, 402, 293
Vauclair S., Théado S., 2004, A&A, 425, 179